Proceedings of the
46th IEEE Conference on Decision and Control
New Orleans, LA, USA, Dec. 12-14, 2007



# Computation of solutions to the Moskowitz Hamilton-Jacobi-Bellman equation under viability constraints

Alexandre M. BAYEN, Christian CLAUDEL, Patrick SAINT-PIERRE

*Abstract*— **This article proposes a new capture basin algorithm for computing the numerical solution of a class of *Hamilton-Jacobi-Bellman* (HJB) *partial differential equations* (PDEs), based on a Lax-Hopf formula. The capture basin algorithm is derived and implemented to perform numerical computations of constrained solutions. The rate of convergence of this first order algorithm is assessed experimentally using an analytical benchmark problem. Finally, its performance is measured with highway data obtained for interstate I80 in California.**

## I. INTRODUCTION

**Background, motivation**. This work is motivated by the *Lighthill-Whitham-Richards* (LWR) *partial differential equation* (PDE), which was historically introduced [20], [24] to model the evolution of vehicle density on highways. It is a first order conservation law with concave flux function (usually referred to as *fundamental diagram* [17], [16]). One difficulty which arises in dealing with the LWR PDE (and to a certain extent with its discretizations such as Godunov schemes [26] or the Daganzo Cell Transmission Model [16]) is the irregularity of its solution, which can exhibit discontinuities (shocks) [23].

**The Moskowitz equation.** In order to alleviate these difficulties, one can use an alternate formulation, identified by Daganzo as the *Moskowitz* function [17]. This function provides an alternate formulation to the classical solution of the LWR PDE: it numbers vehicles as they pass a reference point and it describes the evolution of this number over time and space. Daganzo defines the *Moskowitz surface* as the graph of this function in the $(x, t)$ space. With a sign change, it can be shown that the Moskowitz surface is actually the graph of the solution of a *Hamilton-Jacobi-Bellman* (HJB) PDE, the solution of which also represents the *cumulated vehicle count* between any two points on the highway [22], [17], [26]. The benefit of this formulation is that it transforms the shocks observed in the solutions of the LWR PDE into kinks (non differentiability) in the solution of the corresponding HJB PDE, which are much easier to deal with theoretically and numerically.

**HJB PDEs with concave Hamiltonians.** In the present work, we investigate a class of HJB PDEs with concave Hamiltonians, such as the ones encountered in highway traffic. Inspired by the terminology of Daganzo, we refer to the corresponding HJB PDE as the *Moskowtiz PDE*, and the graph of the corresponding solution the *Moskowitz surface*. We recognize that our definition flips $x$ into $-x$ w.r.t. the definition of Daganzo, but since these two definitions are strictly equivalent, we use the same terminology to refer to both of them.

All our results are presented in the context of highways for illustration purposes, but we want to stress out that our results are very general, and will in fact apply to any HJB PDE with Hamiltonians satisfying the requirements outlined in this article, and thus apply to several other fields such as finance [5], [4]. We base our study on *viability theory* [1], which serves as a mathematical framework to mathematically characterize the proper (viscosity [15], [14] or in this case, Barron-Jensen / Frankowska [7], [18]) solution of the HJB PDE. Existence and uniqueness results for a generalized solution with additional equality constraints are available in [3] to which we refer the reader for the proofs of the results presented in this article.

**Contributions of the article**. The first main contribution of the article (Section II) is the derivation of properties of this class of solutions of HJB PDEs from the properties of capture basins, for which a full length proof is available in [3]. In the present case, with Dirichlet conditions, a Lax-Hopf formula is fully developed in [3] and enables a full characterization of the solution provided by the formulation (10) (Section II-C). For this, several key contributions are needed with the flux function (Hamiltonian), outlined in Section II-B, also available in [3]. The use of the Saint-Pierre viability algorithm to compute and analyze the solutions of the Moskowitz equation is the second contribution of this article. Additionally to the first order convergence rate of the algorithm, we provide experimental evidence of the convergence on a benchmark example which can be solved analytically. We further investigate the influence of both discretization parameters on the error of the numerical computation. We then present some useful control policies based on the upper viability constraints. Finally, Section V presents an implementation of the algorithm on Interstate I80 in California, using PeMS data.

The contributions of this article are in the field of set-valued numerical analysis.

1) It shows the implementation of an improved version of the viability algorithm to a specific problem.
2) It provides experimental evidence of numerical evidence, which is rare in the viability literature.
3) It is the first application of viability theory to real

Assistant Professor, Systems Engineering, Department of Civil and Environmental Engineering, University of California, Berkeley, CA, 94720-1710.

LICIT Laboratory, ENTPE/INRETS, Rue Maurice Audin, 69518 Vaulx-en-velin Cedex, France. claudel@berkeley.edu. Corresponding Author.

Professor, Department of Mathematics, Université Paris-Dauphine, Paris, France.

1-4244-1498-9/07/$25.00 ©2007 IEEE.

traffic data.

## II. Hamilton-Jacobi formulation of the Moskowitz problem

### A. Statement of the problem

The physics of highway traffic flow exhibit two distinct modes to model the evolution of cars on the highway: a *free flow* mode and a *congested* mode [20], [24], [21], [26], [16], [17]. This fact is usually encoded in a *fundamental diagram* [16], which models the flux of cars $\psi(\cdot)$ [in vehicles per unit time], as a function of the local density of cars $\rho$ [in vehicles per unit length]. This empirically measured phenomenological law is usually taken to be concave, with a global maximum. For lower values of density, the highway is said to be uncongested (free flow mode), and for higher values it is said to be congested (congested mode). The simplest model to encode this is the trapezoidal (or in specific cases triangular) fundamental diagram:

**Example —** *Trapezoidal flux function* [16]. One of the simplest fundamental diagram models is the trapezoidal model:

$$\psi(\rho) \;=\; \begin{cases} \nu^\flat \rho & \text{if} \quad \rho \leq \gamma^\flat \\ \delta & \text{if} \quad \rho \in [\gamma^\flat, \gamma^\sharp] \\ \nu^\sharp(\omega-\rho) & \text{if} \quad \rho \geq \gamma^\sharp \end{cases} \tag{1}$$

where $\omega$ is the *jam density*, $\delta \leq \frac{\omega \nu^\flat \nu^\sharp}{\nu^\flat + \nu^\sharp}$ is the maximal flux and $\gamma^\flat := \frac{\delta}{\nu^\flat}$ and $\gamma^\sharp := \frac{\nu^\sharp \omega - \delta}{\nu^\sharp}$ the lower and upper critical densities. When $\gamma^\flat = \gamma^\sharp$, the model is triangular, as used in the Daganzo cell transmission model [16]. □

**Example —** *Greenshields flux function* [19]. Another possible fit for the flux function $\psi(\cdot)$ is called the *Greenshields flux function* and is given by:

$$\psi(\rho) \;=\; \begin{cases} \nu\rho & \text{if} \quad \rho \leq 0 \\ \frac{\nu}{\omega}\rho(\omega-\rho) & \text{if} \quad \rho \in [0,\omega] \\ \nu(\omega-\rho) & \text{if} \quad \rho \geq \omega \end{cases} \tag{2}$$

where $\nu$ is the *free flow velocity.* □

**The Moskowitz function.** The slope of $\psi$ determines the modes in which the system is locally in (congested or free flow), which in the triangular case leads to a forward or backward propagating wave.

In order to alleviate the technical difficulties resulting from shocks present in solution of the LWR PDE, an alternate formulation consists in considering the *cumulated number of vehicles*, widely used in the transportation literature as well [22]. The cumulative number of vehicles can be thought of as a primitive of the density over space. Setting $X := \mathbb{R}$ and $K := [\xi, +\infty[$, $\psi$ a concave flux function vanishing at density 0 and at a jam density $\omega > 0$, the function

$$\mathbf{N}(t,x) \;:=\; \int_\xi^x \rho(t,u)du$$

is the cumulated number of vehicles at time $t$ and at location $x \in K$. It satisfies by construction the Dirichlet condition $\forall\; t \geq 0, \quad \mathbf{N}(t,\xi) \;=\; 0$. It is linked to the *Moskowitz function* by a $x \to -x$ variable change and a vertical shift (see Daganzo [17]). Formally, the evolution of the cumulated number $\mathbf{N}(t,x)$ of vehicles is the solution of an *Hamilton-Jacobi-Bellman* (HJB) PDE of the form:

$$\frac{\partial \mathbf{N}(t,x)}{\partial t} + \psi\left(\frac{\partial \mathbf{N}(t,x)}{\partial x}\right) \;=\; \psi(v(t)) \tag{3}$$

where the flux function $\psi$ appearing in this HJB PDE is the empirically measured flux function of the LWR PDE [20], [24], [6], [26] (for example the two functions $\psi$ presented before). The function $v(\cdot)$ will be regarded as a control of the HJB PDE in forthcoming studies. It could for example model the inflow of vehicles at the entrance of a stretch of highway. It is considered as a given datum (controllable though) in this paper. The solution of this HJB PDE is upper semicontinuous and is not necessarily differentiable. Actually, the non differentiability of the cumulated number of vehicles is closely related to the presence of the shocks of the solution to the LWR PDE [11], [12], [13].

**Assumptions.** We posit the following assumptions

1) A concave function $\psi : X \mapsto \mathbb{R}$ on $[0,\omega]$, which vanishes at 0 and $\omega$, equal to $\psi'(0)v$ for $v \leq 0$ and $\psi'(\omega)(\omega - v)$ for $v \geq \omega$.
2) A bounded continuous function $v : \mathbb{R}_+ \mapsto \mathrm{Dom}(\psi)$,
3) An upper semicontinuous initial datum $\mathbf{N}_0 : X \mapsto \mathbb{R}_+$. We set $\mathbf{N}_0(0,x) := \mathbf{N}_0(x)$ and $\mathbf{N}_0(t,x) := -\infty$ if $t > 0$.
4) A Lipschitz function $\mathbf{b} : \mathbb{R}_+ \times X \mapsto \mathbb{R} \cup \{-\infty\}$ setting the upper constraint.

**Problem statement.** Under the above mentioned assumptions, that are assumed all along this paper, we shall solve the existence of a solution to the *non-homogenous HJB PDE:*

$$\forall\, t > 0, \;\; x \in \mathrm{Int}(K), \;\; \frac{\partial \mathbf{N}(t,x)}{\partial t} + \psi\left(\frac{\partial \mathbf{N}(t,x)}{\partial x}\right) \;=\; \psi(v(t)) \tag{4}$$

satisfying the *initial and Dirichlet conditions*

$$\begin{cases} (i) & \forall\, x \in K, \;\; \mathbf{N}(0,x) = \mathbf{N}_0(x) \text{ (initial condition)} \\ (ii) & \forall\, t \geq 0, \;\; \mathbf{N}(t,\xi) = 0 \text{ (Dirichlet boundary condition)} \end{cases} \tag{5}$$

and the user defined *viability constraints*

$$\forall\, t \geq 0, \; x \in K, \;\; \mathbf{N}(t,x) \;\leq\; \mathbf{b}(t,x) \tag{6}$$

(upper inequality constraint)

### B. Flux functions

The assumption that the flux function $\psi$ is concave and upper semicontinuous plays a crucial role for defining the viability hyposolution. Indeed, since $\psi$ is concave, the function $\varphi(p) := -\psi(p)$ is convex and its Fenchel transform is defined by:

$$\varphi^*(u) \;:=\; \sup_{p \in \mathrm{Dom}(\varphi)} [p \cdot u - \varphi(p)] \;=\; \sup_{p \in \mathrm{Dom}(\psi)} [p \cdot u + \psi(p)] \tag{7}$$

Recall that the fundamental theorem of convex analysis states that $\varphi = \varphi^{**}$ if and only if $\varphi$ is convex, lower semicontinuous, and non trivial (i.e. $\mathrm{Dom}(\varphi) := \{p \mid \varphi(p) < +\infty\} \neq \emptyset$). Therefore we can recover the function $\psi$ from $\varphi^*$ by

$$\psi(p) \;:=\; \inf_{u \in \mathrm{Dom}(\varphi^*)} [\varphi^*(u) - p \cdot u] \tag{8}$$

Let us consider a concave flux function $\psi_0$ defined on a neighborhood of the interval $[0,\omega]$ and satisfying

$$\psi(0) \;=\; \psi(\omega) \;=\; 0$$

We assume for simplicity that $\psi$ is differentiable at 0 and $\omega$, and we set $\nu^\flat = \psi'(0) \geq 0$ and $\nu^\sharp = -\psi'(\omega) \geq 0$ We associate with it the continuous concave function $\psi$ defined by

$$\psi(p) \;=\; \left\{ \begin{array}{lll} \nu^\flat p & \text{if} & p \leq 0 \\ \psi_0(p) & \text{if} & p \in [0,\omega] \\ \nu^\sharp(\omega - p) & \text{if} & p \geq \omega \end{array} \right.$$

Then the Fenchel transform $\varphi^*$ satisfies

$$\varphi^*(u) \;=\; \left\{ \begin{array}{lll} \varphi^*(u) & \text{if} & u \in [-\nu^\flat, +\nu^\sharp] \quad \mathrm{Dom}(\phi^*) \\ +\infty & \text{if} & u \notin [-\nu^\flat, +\nu^\sharp] \quad \mathrm{Dom}(\phi^*) \end{array} \right.$$

and is bounded above.

**Example —** *trapezoidal flux function* — For this function, the Fenchel transform is equal to

$$\varphi^*(u) \;=\; \left\{ \begin{array}{lll} \frac{\delta}{\nu^\flat} u + \delta & \text{if} & u \in [-\nu^\flat, 0] \\ \dfrac{(\omega\nu^\sharp - \delta)}{\nu^\sharp} u + \delta & \text{if} & u \in [0, +\nu^\sharp] \\ +\infty & \text{if} & u \notin [-\nu^\flat, +\nu^\sharp] \end{array} \right.$$

It is piecewise affine (affine on $[-\nu^\flat, 0]$ and $[0, +\nu^\sharp]$) and satisfies $\varphi^*(0) = \delta$. The superdifferential $\partial_+\psi(p)$ is equal to

$$\partial_+\psi(p) \;=\; \left\{ \begin{array}{lll} \nu^\flat & \text{if} & p \leq \gamma^\flat \\ 0 & \text{if} & p \in [\gamma^\flat, \gamma^\sharp] \\ -\nu^\sharp & \text{if} & p \geq \gamma^\sharp \end{array} \right.$$

and thus, piecewise constant. □

**Example —** *Greenshields flux function* — From (2), the Greenshields function is given by: $\psi_0(p) \;:=\; \frac{\nu}{\omega} p(\omega - p)$. Hence, its Fenchel transform $\varphi^*$ is equal to

$$\varphi^*(u) \;=\; \left\{ \begin{array}{lll} \frac{\omega}{4\nu}(u+\nu)^2 & \text{if} & u \in [-\nu, +\nu] \\ +\infty & \text{if} & u \notin [-\nu, +\nu] \end{array} \right.$$

The maximum flux is equal to $\varphi^*(0) = \frac{\omega\nu}{4}$. □

### C. Viability hyposolution of the HJB equation

We define a target $\mathcal{C} := \mathcal{H}yp(\mathbf{c})$ as the subset of triples $(T,x,y) \subset \mathbb{R}_+ \times X \times \mathbb{R}$ such that $y \leq \mathbf{c}(T,x)$ (which is the *hypograph* of the function $\mathbf{c}$), where the function $\mathbf{c}(t,x)$ is defined (here) by:

$$\mathbf{c}(t,x) \;:=\; \left\{ \begin{array}{lll} -\infty & \text{if} & t > 0 \text{ and } x > \xi \\ \mathbf{N}_0(x) & \text{if} & t = 0 \text{ and } x \geq \xi \\ 0 & \text{if} & t \geq 0 \text{ and } x = \xi \end{array} \right.$$

The environment $\mathcal{K} := \mathcal{H}yp(\mathbf{b})$ is the subset of triples $(T,x,y) \subset \mathbb{R}_+ \times X \times \mathbb{R}$ such that $y \leq \mathbf{b}(T,x)$, which is a user-defined function (this is the *hypograph* of the function $\mathbf{b}$). We define the auxiliary control system $(F)$:

$$\left\{ \begin{array}{lll} \tau'(t) &=& -1 \\ x'(t) &=& u(t) \qquad\qquad\qquad u(t) \;\in \mathrm{Dom}(\varphi^*) \\ y'(t) &=& \varphi^*(u(t)) - \psi(v(\tau(t))) \end{array} \right. \tag{9}$$

where $\varphi^*$ is the Fenchel conjugate function of $\psi$, as defined previously. To be rigorous, we have to mention *once and for all* that the controls $u(\cdot)$ are measurable integrable functions with values in $\mathrm{Dom}(\varphi^*)$, and thus, ranging $L^1(0,\infty;\mathrm{Dom}(\varphi^*))$, and that the above system of differential equations is valid for almost all $t \geq 0$.

**The Viability Hyposolution.** The capture basin $\mathrm{Capt}_{(F)}(\mathcal{K},\mathcal{C})$ of a target $\mathcal{C}$ viable in the environment $\mathcal{K}$ under the control system $(F)$ is the subset of initial states $(t,x,y)$ such that there exists a measurable control $u(\cdot)$ such that the associated solution

$$s \mapsto \left( t-s, x + \int_0^s u(\tau)d\tau, y + \int_0^s (\varphi^*(u(\tau)) - \psi(v(t-\tau)))d\tau \right)$$

to the system $(F)$ is viable in $\mathcal{K} = \mathcal{H}yp(\mathbf{b})$ until it reaches the target $\mathcal{C} = \mathcal{H}yp(\mathbf{c})$. The *viability hyposolution* $\mathbf{N}$ is defined by

$$\mathbf{N}(t,x) \;:=\; \sup_{(t,x,y) \in \mathrm{Capt}_{(F)}(\mathcal{K},\mathcal{C})} y \tag{10}$$

Our main contribution in this article states that the hypograph of the Moskowitz solution is the capture basin of the target $\mathcal{C}$ viable in the environment $\mathcal{K}$ under the auxiliary system (F).

**Non-homogenous Dirichlet/Initial value Problem with inequality contraints.** The viability hyposolution $\mathbf{N}$ defined by (10) is the *largest* upper semicontinuous solution to HJB PDE(4) satisfying initial and Dirichlet conditions (5) and inequality constraints (6). If the functions $\psi$, $\varphi^*$ and $v$ are furthermore Lipschitz, then the viability hyposolution $\mathbf{N}$ is its *unique* upper semicontinuous solution in both the contingent Frankowska sense and in the Barron-Jensen/Frankowska sense. The proof of this theorem is available in [3], as well as the precise definitions of the corresponding hyposolutions in the sense of Barron, Jensen and Frankowska.

## III. Viability algorithm for the Moskowitz PDE

**The capture basin algorithm for the Moskowitz PDE**. The second major contribution of this article is the formulation of the Saint-Pierre capture basin algorithm for the Moskowitz PDE. The precise description of the algorithm and its implementation is outside the scope of this conference article. We use this algorithm to solve the Moskowitz PDE with and without constraints.

The Saint-Pierre algorithm is adapted to the case in which the target $\mathcal{C}$ and the environment $\mathcal{K}$ are hypographs, which allows us to take some specificities of the problem into account. It differs from a finite difference scheme [26] because of the use of the Fenchel transform $\varphi^*$ instead of the function $\psi$. Above all, it includes the possibility of constraints on the solution with the function $\mathbf{b}(t,x)$, which, to our best knowledge, standard HJB algorithms do not provide. Some examples of constrained solutions are depicted in section IV. These examples clearly show that the constrained solution is not the supremum of the the constraint $\mathbf{b}(t,x)$ and the unconstrained solution.

**Illustration of the convergence properties of the algorithm.** A theoretical first order convergence rate of the Saint-Pierre algorithm is established in [10] for the numerical computation of value functions; in [10] the proper notion

of convergence (also valid for the present algorithm) is *hypographical convergence*. Typically, a convergence rate $\alpha$ of the Saint-Pierre algorithm means that the error is proportional to $h^\alpha$, where $h$ is the space discretization step. Even though the convergence of the present algorithm can be established theoretically based on [10] (see [5], [4] for similar applications in finance), it is useful to assess how fast this convergence happens in practice. For this, we use the benchmark example previously used for the LWR PDE in [8], adapted by integration for the Moskowitz PDE. The benchmark example is a full analytical solution of the LWR PDE, including multiple shocks and expansion waves, obtained with the method of characteristics. The corresponding analytical solution of the Moskowitz PDE (3) can be obtained by integration over space. The parameters used in this study are $\nu = 1$ and $\omega = 4$ for a Greenshields flux function (see [8], [3] for more details). The $L_1$ and $L_2$ relative errors are computed by comparison between the analytical expression of $N(t,x)$ for the benchmark example and the numerical computation of the solution returned by the viability algorithm:

$$\text{Error}_{L_n} := \left( \frac{\sum_{(t_h,x_h)\in \text{grid}} |\mathbf{N}_h(t_h,x_h) - \mathbf{N}(t_h,x_h)|^n}{\sum_{(t_h,x_h)\in \text{grid}} |\mathbf{N}(t_h,x_h)|^n} \right)^{\frac{1}{n}}$$

for $n = 1, 2$. In this formula, $N_{\text{total}}$ is the total number of points $(t_h, x_h)$ on the computational grid, $\mathbf{N}_h$ the numerical result, and $\mathbf{N}$ the analytical result to be used for the comparison. The error plots are depicted in Figure 1 for both norms which shows empirical evidence of the first order convergence rate in the $L_1$ and $L_2$ sense. A least square fit provides the following convergence rates: $\alpha = -1.15$ and $\alpha = -1.07$ for $L_1$ and $L_2$ respectively.

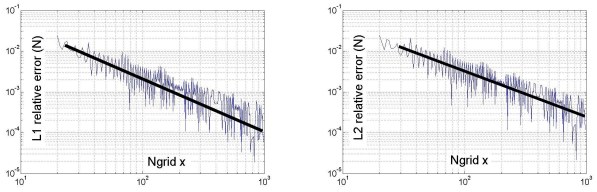


Fig. 1. Evolution of $L_1$ (left) and $L_2$ (right) relative errors on $N(t,x)$ versus $N_{\text{grid}_x}$ The continuous lines indicate the best power fit of $L_1$ and $L_2$.

**Influence of the choice of the discretization parameters**. Finite difference methods require the discretization parameters to satisfy a *Courant-Friedrichs-Levy* (CFL) condition [8], [26] in order to obtain convergence. In the same way, viability schemes require a similar condition (see [25], [9] for example). The convergence rate of our algorithm is assessed numerically as a function of the respective values of our discretization parameters $N_{\text{grid}_t}$ and $N_{\text{grid}_x}$ in the $x$ and $t$ variables. As can be seen in Figure 2, the lowest possible error (dark gray areas) is obtained when $N_{\text{grid}_t} \to 0$. Nevertheless, the convergence condition for the algorithm does not imply that using a larger $\Delta t$ provides a better accuracy for a lower computational cost. Since the number

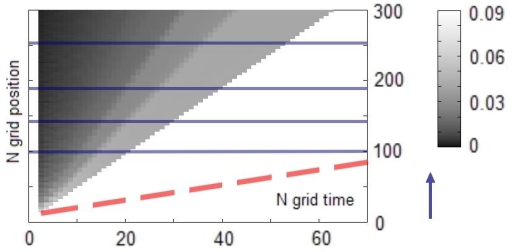


Fig. 2. Evolution of the $L_1$ relative error of $N(t,x)$ versus $N_{\text{grid}_t}$ and $N_{\text{grid}_x}$.

of iterations of the algorithm is proportional to $\Delta t$, the viability algorithm requires the same amount of computations whatever the value of $\Delta t$ is. Lines of equal computational cost (thin lines) are also shown as well as the direction of higher computation cost (arrow). We also plotted in Figure 2 the CFL condition $(\nu^\sharp + \nu^\flat) \cdot \Delta t = \Delta x$ (dashed thick line) used in the framework of the Godunov numerical scheme [8], [26], for comparison purposes.

**Formal links with the LWR PDE.** Finally, the algorithm can also be used to compute the density $\rho(t,x)$ from the cumulated count $\mathbf{N}(t,x)$. Note that alternate viability algorithms have also been developed to compute this density directly, for example [2].

When the flux function is differentiable on $[0,\omega]$, we can compute the density $\rho(t,x)$ using the following property:

$$u_{\text{opt}}(t,x) \in -\partial_+\psi(\rho(t,x)) \;=\; -\left(\frac{\partial\psi(a)}{\partial a}\right)_{a=\rho(t,x)}$$

$u_{\text{opt}}(t,x)$ corresponds to the value of the pseudo control $u$ at position $x$ and time $t$ which maximizes $\varphi^*(u(t)) - \psi(v(\tau(t)))$. Hence, using elements of convex analysis, we obtain:

$$\rho(t,x) = \left(\frac{\partial\varphi^*(u)}{\partial u}\right)_{u=u_{\text{opt}}(t,x)}$$

Using the Greenshields Flux Function, which is differentiable on $[0,\omega]$, we plot the density profile associated to $\mathbf{N}(t,x)$ in Figure 3.

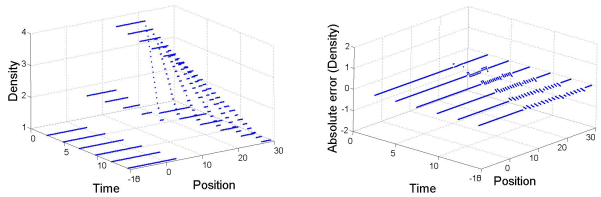


Fig. 3. Density derived from the optimal values of the pseudo-control, using the Greenshields Flux Function. **Left:** Computation of the density. **Right:** Difference between the numerically derived density and the analytically computed density.

Using the trapezoidal flux function, which is not differentiable in both $\gamma^\flat$ and $\gamma^\sharp$, we can only obtain $\rho(t,x) \in \partial_+\varphi^*(u_{\text{opt}}(t,x))$. This formula enables us to

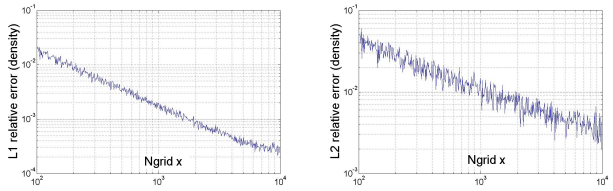


Fig. 4. Evolution of $L_1$ and $L_2$ relative errors on density versus $N_{\text{grid}_x}$

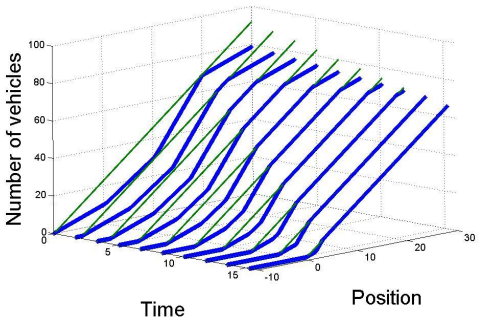


Fig. 5. Constrained solution to the benchmark example extracted from [8]. The affine function (decreasing with time) constraining the solution is shown (thin line) as well as the constrained solution (thick line).

obtain a set valued map containing the graph of $\rho(t,x)$, but not the graph of $\rho(t,x)$ itself.

However, since $\rho(t,x) = \frac{\partial \mathbf{N}(t,x)}{\partial x}$, we can also compute $\rho(t,x)$ using the following finite difference scheme:

$$\rho(t,x) = \frac{\mathbf{N}(t,x+\Delta x) - \mathbf{N}(t,x)}{\Delta x}$$

Even though numerical differentiation with finite difference schemes in general provides poor results, the results obtained with this scheme are strikingly good. Figure 4 summarizes the evolution of the $L_1$ and $L_2$ errors on density versus $N_{\text{grid}_x}$, for a constant $\Delta t$ (thus constant $N_{\text{grid}_t}$).

## IV. Constrained solutions to the HJB equation

Viability theory enables us to set upper constraints on the solution to the HJB equation. Note that there is a unique solution to the HJB equation with constraints, and this solution does not follow the HJB equation in $(t,x)$ if $\mathbf{N}(t,x) = \mathbf{b}(t,x)$. We can also set on the viability solution any upper constraint $\mathbf{b}(t,x)$ satisfying the consistency conditions exposed in [3].

Figure 5 displays the constrained solution associated to the benchmark example from [8]. The upper constraint function $\mathbf{b}(t,x)$ is affine (w.r.t. to position) and decreasing with time, in order to constrain the average density between the last vehicle and any vehicle to a given upper limit $\overline{\rho}$. This constraint can be regarded as a control of the traffic flow.

An alternate way to visualize the effects of the constraints on the solution is to compute the vehicles trajectories. Since $v(\cdot) = 0$, the trajectory of vehicle number $\overline{N}$ is solution to the equation $\mathbf{N}(t,x) = \overline{N}$. The trajectories of vehicles number 10 (bottom), 20, 30, 40, 50 and 60 (top) are shown in both cases (constrained and unconstrained) in Figure 6.

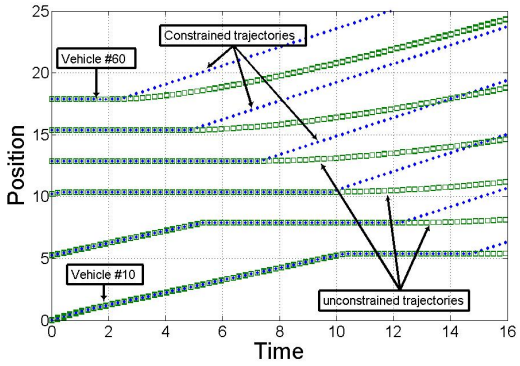


Fig. 6. The dotted lines correspond to the trajectories associated to the constrained solution (shown in Figure 5). For comparison purposes, we also plotted the unconstrained trajectories of the same vehicles (squares) .

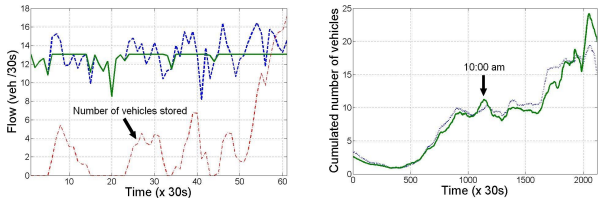


Fig. 7. **Left:** Flow-time curves. The (actual) measured inflow on the boundary $x = \xi$ is represented by the dashed curve. The continuous curve shows the simulated inflow through boundary $x = \xi$, taking into account the highway capacity. The number of corresponding (remaining) vehicles stored at the $x = \xi$ boundary is shown on the dash dotted curve. **Right:** Comparison between experimental values and simulated values for the cumulated vehicle number $\mathbf{N}(t, \xi + L)$ between $\xi$ and $L$.

## V. Implementation on I80 using PeMS data

We use the same experimental set up as in earlier work [26] to assess the performance of the algorithm with highway traffic data: we use three loop detectors in Interstate I80 at Emeryville (see [26] for a map of the area). As usual when dealing with inflow and outflow conditions in the presence of weak boundary conditions, we prescribe inflows and outflows only when the characteristics of the system enter the computational domain [6], [26]. We simulate a portion of the highway between two inductive loop detectors on Interstate I80. When the measured inflow (upstream) exceeds the modeled highway capacity (because of noise in the measurements or model inaccuracy), we "store" the corresponding vehicles at $x = \xi$ until they can be released into the highway. The resulting curves are shown in Figure 7 (left): the cutoff happens at $\psi(v(t)) = \delta$ above which the vehicles have to be stored until the highway capacity allows them to enter at $x = \xi$.

In this figure, as well as in the subsequent ones, all numbers of vehicles are per lane. All times are given in 30 s. increments. The corresponding number of "stored" vehicles is shown in the same subfigure, and the corresponding $\mathbf{N}(\xi+L,t)$ curves are shown in the right subfigures, where $L$ represents the length of the corresponding highway stretch. The evolution $\mathbf{N}(\xi + L, t)$ thus represents the evolution of

the cumulated number of vehicles between $\xi$ and $\xi + L$ as a function of time. Both simulated and measured curves are represented on this plot and show remarkable agreement. The differences between simulation and theory are mainly linked with uncertainties on the numerical values of the parameters of the model.

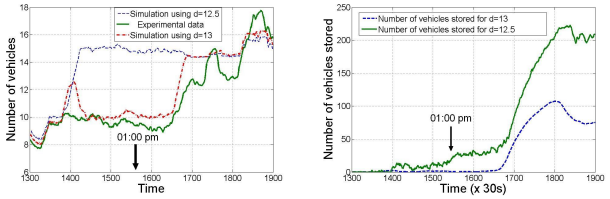


Fig. 8. **Evolution of the simulated results for a small variation of $\delta$.** The left subplot represents the simulated cumulated number of vehicles when considering $\delta = 12.5$ (dashed) and $\delta = 13$ (dash dotted). The actual values are represented by the continuous curve. The right subplots shows the evolution total number of vehicles stored at the $x = \xi$ boundary considering $\delta = 12.5$ (continuous) and $\delta = 13$ (dashed).

Figure 8 shows that a small modification of the parameter $\delta$ (representing the capacity of the freeway in the model) can lead to considerable variations of the solution. In this figure, a bottleneck appears for $t \geq 1400$ if we set $\delta = 12.5$, whereas the freeway remains in free-flow mode until $t = 1650$ if we set $\delta = 13$. The left subplot in Figure 8 represents the number of vehicles stored at the $x = \xi$ boundary, for $\delta = 12.5$ and $\delta = 13$. If we chose $\delta = 12.5$, vehicles are stockpiled at the $x = \xi$ boundary when $t \geq 1400$ because the lack of capacity triggers a congestion which lowers again the remaining capacity of the freeway. This congestion does not appear if we slightly increase $\delta$ to $\delta = 13$, and the freeway remains in free flow mode in this case (for $1400 \geq t \geq 1650$). This simulation shows us that the evolution of the cumulated vehicle count on the highway is very sensitive to the choice of $\delta$: the traffic mode can switch easily between the free-flow mode and the congested mode when the inflow is close to $\delta$.

## ACKNOWLEDGMENTS

The authors wish to thank Issam Strub for helping with the I80 data used for this study, and Jean-Baptiste Lesort for helping with the interpretation of the experimental data.

## REFERENCES

[1] J.-P. AUBIN. *Viability Theory*. Birkhäuser, Boston, MA, 1991.

[2] J.-P. AUBIN, A. M. BAYEN, and P. SAINT-PIERRE. A viability approach to Hamilton-Jacobi equations: application to concave highway traffic flux functions. In *44th IEEE Conference on Decision and control and European Control Conference*, pages 3519–3524, Sevilla, Spain, Dec 2005.

[3] J.-P. AUBIN, A. M. BAYEN, and P. SAINT-PIERRE. Dirichlet problems for some Hamilton-Jacobi equations with inequality constraints. Technical report, Scuola Normale Superiore, Pisa, Italy, May 2006. Preprint di Matematica, no. 4.

[4] J.-P. AUBIN, D. PUJAL, and P. SAINT-PIERRE. Dynamic management of portfolios with transaction costs under tychastic uncertainty. In Ben-Ameur and Breton, editors, *Numerical Methods in Finance*. Kluwer, New York, NY, 2005.

[5] J.-P. AUBIN and P. SAINT-PIERRE. A tychastic approach to guaranteed pricing and management of portfolios under transaction constraints. In *Proceedings of the 2005 Ascona Conferences on Stochastic Analysis, Random Fields and Applications, Progress in Probability*, 2006.

[6] C. BARDOS, A. Y. LEROUX, and J. C. NEDELEC. First order quasilinear equations with boundary conditions. *Communications in partial differential equations*, 4(9):1017–1034, 1979.

[7] E. N. BARRON and R. JENSEN. Optimal control and semicontiuous viscosity solutions. *Proceedings of the American Mathematical Society*, 113:393–402, 1991.

[8] A. M. BAYEN, R. L. RAFFARD, and C. TOMLIN. Network congestion alleviation using adjoint hybrid control: Application to highways. Number 1790 in Lecture Notes in Computer Science, pages 95–110. Springer Verlag, 2004.

[9] P. CARDALIAGUET, M. QUINCAMPOIX, and P. SAINT-PIERRE. Set-valued numerical analysis for optimal control and differential games. In M. Bardi, T.E.S. Raghavan, and T. Parthasarathy, editors, *Stochastic and Differential Games: Theory and Numerical Methods*, Annals of the International Society of Dynamic Games. Birkhäuser, Boston, MA, 1999.

[10] P. CARDALIAGUET, M. QUINCAMPOIX, and P. SAINT-PIERRE. Numerical schemes for dicontinuous value functions of optimal control. *Set-Valued Analysis*, 8(1-2):111–126, 2000.

[11] N. CAROFF and H. FRANKOWSKA. Optimality and characteristics of hamilton-jacobi-bellman equations. volume 107 of *International Series of Numerical Mathematics*, pages 169–180. 1992.

[12] N. CAROFF and H. FRANKOWSKA. A note on conjugate points and shocks in nonlinear optimal control. *Bull. of the Polish Academy of Sciences*, 42:115–128, 1994.

[13] N. CAROFF and H. FRANKOWSKA. Conjugate points and shocks in nonlinear optimal control. *Transactions of the AMS*, 348:3133–3153, 1996.

[14] M. G. CRANDALL, L. C. EVANS, and P.-L. LIONS. Some properties of viscosity solutions of Hamilton-Jacobi equations. *Transactions of the American Mathematical Society*, 282(2):487–502, 1984.

[15] M. G. CRANDALL and P.-L. LIONS. Viscosity solutions of Hamilton-Jacobi equations. *Transactions of the American Mathematical Society*, 277(1):1–42, 1983.

[16] C. DAGANZO. The cell transmission model: a dynamic representation of highway traffic consistent with the hydrodynamic theory. *Transportation Research*, 28B(4):269–287, 1994.

[17] C. DAGANZO. On the variational theory of traffic flow: well posedness, duality and applications. *Networks and Heterogeneous Media*, 1(4):601–619, 2006.

[18] H. FRANKOWSKA. Lower semicontinuous solutions of Hamilton-Jacobi-Bellman equations. *SIAM Journal on Control and Optimization*, 31:257–272, 1993.

[19] B. D. GREENSHIELDS. A study of traffic capacity. *Proceedings of the Highway Research Board*, 14:448–477, 1935.

[20] M. J. LIGHTHILL and G. B. WHITHAM. On kinematic waves. II. A theory of traffic flow on long crowded roads. *Proceedings of the Royal Society of London*, 229(1178):317–345, 1956.

[21] L. MUNOZ, X. SUN, G. GOMES, and R. HOROWITZ. Methodological calibration of the cell transmission model. In *2004 American Control Conference*, pages 798–803, Boston, MA, June 2004.

[22] G. F. NEWELL. A simplified theory of kinematic waves in highway traffic, part I: general theory. *Transporation Research B*, 27B(4):281–287, 1993.

[23] O. A. OLEINIK. On discontinuous solutions of nonlinear differential equations. *Uspekhi Mat. Nauk.*, 12:3–73, 1957. English translation: *American Mathematical Society*, Ser. 2 No. 26 pp. 95–172, 1963.

[24] P. I. RICHARDS. Shock waves on the highway. *Operations Research*, 4(1):42–51, 1956.

[25] P. SAINT-PIERRE. Approximation of the viability kernel. *Applied Mathematics and Optimization*, 29:187–209, 1994.

[26] I. S. STRUB and A. M. BAYEN. Weak formulation of boundary conditions for scalar conservation laws. *International Journal on Nonlinear and Robust Control*, 16(16):733–748, Nov. 2006.